

Is altermagnetism in vanadium oxychalcogenides a lost cause?

Bishal Thapa,^{1,2,*} Po-Hao Chang,^{1,2,†} Kirill Belashchenko,^{3,‡} and Igor I. Mazin^{1,2,§}

¹George Mason University, Department of Physics and Astronomy

²Quantum Science and Engineering Center, Fairfax, USA

³Department of Physics and Astronomy and Nebraska Center for Materials and Nanoscience, University of Nebraska-Lincoln, Lincoln, Nebraska 68588, USA

Vanadium-based oxychalcogenide compounds with the inverse Lieb-lattice (ILL) structural pattern have been recently proposed as candidate altermagnets (AM). However, early studies postulated ferromagnetic interlayer coupling, a critical requirement for preserving the bulk AM state. Here we present a systematic survey of the complete AV_2Q_2O family ($A = K, Rb, Cs$; $Q = S, Se, Te$) in terms of their magnetic ordering and interlayer coupling. While *intralayer* exchange interaction favors AM ordering in a single ILL layer across the entire family, the relatively weak *interlayer* coupling in most cases favors Kramers-degenerate antiferromagnetic order with a doubled magnetic unit cell. This means that most stoichiometric bulk materials, including the previously proposed candidate KV_2Se_2O , are not altermagnetic, with CsV_2Te_2O being the only exception. Using hole doping to simulate alkali vacancies, we show that realistic deviations from stoichiometry do not change the magnetic ground state in these compounds.

Introduction — Altermagnetism (AM) has emerged as a frontier in contemporary condensed matter physics [1–7] and spintronics, offering the prospect of generating large spin splittings of nonrelativistic origin on the order of electronvolts in the absence of net magnetization [8, 9]. This remarkable property positions altermagnetic materials as promising candidates for next-generation spintronic applications [10–14].

Inverse Lieb lattice (ILL) compounds have attracted considerable attention as a versatile platform for hosting altermagnetic states [15–20]. Their appeal stems from several key features: natural abundance of the constituent elements, *d*-wave altermagnetic spin-splitting symmetry, availability of metallic compounds [18, 19], and directionally distinct second-nearest-neighbor exchange paths potentially leading to large chiral magnon splitting [20]. The characteristic architecture of ILL compounds — comprising transition-metal (TM) layers decorated by ligand atoms and separated by various filler layers — provides highly tunable electronic and magnetic properties, including metallicity, Fermi surface, and Néel temperature T_N . However, altermagnetism is not a universal feature of ILL-based materials, necessitating systematic investigation of the magnetic order in this family [20–23].

We have previously studied *intralayer* magnetic ordering in a broad range of ILL systems, revealing intriguing patterns in AM stabilization [20]. The analysis of these compounds uncovered a potentially significant correlation: transition metals with less than half-filled $3d$ shells exhibit stronger propensity for in-plane altermagnetic order. While a unified microscopic explanation for this trend remains elusive (only a special case of the $3d^5$ $La_2O_3Mn_2Se_2$ compound has been discussed in detail [24]), this observation could provide valuable guidance for identifying promising AM candidates.

Among the experimentally characterized AM candi-

dates, there are two metallic systems belonging to the ILL family, which are both vanadium-based materials with T_N around room temperature [18, 19]. In addition, insulating V_2Se_2O , which consists of similar ILL layers without any intercalating filler layers, has also been synthesized [25]. Its magnetic ordering has not yet been determined experimentally, but theoretical calculations suggest an AM ground state [26, 27]. These observations collectively suggest that vanadium-based ILL compounds are prime candidates for the technologically desirable metallic *d*-wave AM [20].

However, AM of bulk ILL compounds hinges on a critical issue that has not been systematically addressed: the ILL layers must be stacked ferromagnetically along the *c* axis; otherwise, the magnetic unit cell is doubled, and the compound becomes a conventional collinear antiferromagnet with Kramers-degenerate band structure. Many earlier theoretical analyses have either focused on hypothetical monolayer systems or assumed ferromagnetic interlayer coupling [18, 28–30], thus leaving the AM character unresolved for the existing material candidates.

In this paper, guided by the available experimental data [31, 32], we present a systematic survey of the magnetic properties across the complete family of metallic vanadium-based ILL compounds with the general formula AV_2Q_2O , where $A = K, Rb, Cs$ and $Q = S, Se, Te$, focusing on interlayer exchange coupling. This family represents an ideal testbed for several reasons. First, according to our earlier analysis [20], vanadium with its less than half-filled $3d$ shell should form ILL layers with *intralayer* AM, and we can systematically explore the effect of the alkali metal filler (*A*) and chalcogen ligand (*Q*) on the *interlayer* magnetic ordering. Second, they are all metallic. Third, several of these compounds have already been synthesized and structurally characterized, making the whole family experimentally accessible.

In agreement with our earlier results [20], the intralayer

exchange coupling strongly favors monolayer AM in all nine compounds. However, we find that much weaker interlayer exchange coupling favors antiferromagnetic (AF) stacking in all cases except $\text{CsV}_2\text{Te}_2\text{O}$, excluding AM order in all but this one (hypothetical) compound. This conclusion is in contradiction with the original claim that $\text{KV}_2\text{Se}_2\text{O}$ is AM [18] but in agreement with the recent neutron diffraction experiment [33]. We have also checked that this conclusion is robust with respect to a reasonable charge doping, which represents deviations from stoichiometry and incomplete population of the alkali-atom sited in the intercalating layers, such as Rb layers in $\text{Rb}_{1-\delta}\text{V}_2\text{Te}_2\text{O}$ [19].

The rest of this paper is organized as follows. Section II briefly describes the crystal and magnetic structure of the $\text{AV}_2\text{Q}_2\text{O}$ compounds. Section III details the computational methodology. Section IV presents the main results for the exchange coupling in both stoichiometric and hole-doped compounds. Section V concludes the paper.

Crystal and magnetic structure — The compounds in the isoelectronic $\text{AV}_2\text{Q}_2\text{O}$ family ($A = \text{K, Rb, Cs}$; $Q = \text{S, Se, Te}$) crystallize in the primitive tetragonal space group $P4/mmm$ (No. 123), with the experimental lattice constants are reported in Ref. [31]. The A, V, Q, and O atoms occupy the $1b$, $2f$, $2h$, and $1a$ Wyckoff sites, respectively. This structure consists of well-separated $\text{V}_2\text{Q}_2\text{O}$ layers stacked without a lateral shift along the crystallographic c axis and interleaved by layers of alkali-metal ions. The V atoms within each layer form an ILL, as shown in Fig. 1.

The exchange coupling and magnetic ordering within the ILL layer were studied in detail in Ref. 20. The relevant intralayer exchange parameters J_1 , $J_{2\alpha}$, $J_{2\beta}$, and J_3 are indicated in Fig. 1(b). As explained below, in all studied compounds, these parameters reliably stabilize AM order within an isolated ILL monolayer, in agreement with the conclusions of Ref. 20. Our central focus will, therefore, be on the *interlayer* interaction, denoted J_\perp in Fig. 1(c-d), which couples V spins in the adjacent $\text{V}_2\text{Q}_2\text{O}$ layers. Instead of calculating individual pair exchange parameters connecting V atoms in such adjacent layers, we will study the total interlayer coupling using total energy calculations for FM and AF layer stackings, as shown in Fig. 1(c) and 1(d), respectively. A compound with ferromagnetic stacking of Fig. 1(c) is AM, while AF stacking of Fig. 1(d) is a conventional antiferromagnet with a doubled magnetic unit cell.

Computational details — Most first-principles calculations were performed using the numerical-orbital-based density functional theory (DFT) code OpenMX [34, 35]. Core electrons were treated using norm-conserving pseudopotentials [36, 37]. The Perdew–Burke–Ernzerhof (PBE) generalized gradient approximation was employed to describe exchange–correlation effects [38]. Pseudatomic basis functions and pseudopotentials for the

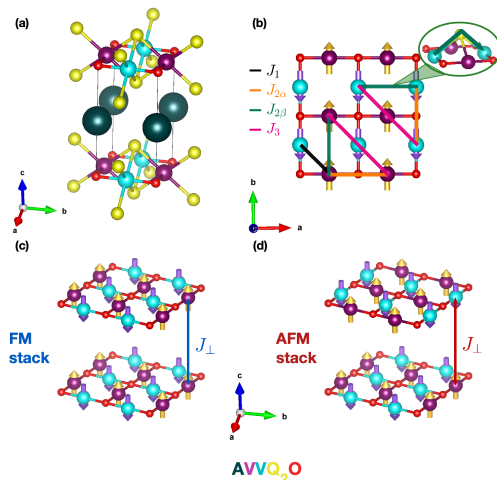


FIG. 1: (a) Crystal structure of $\text{AV}_2\text{Q}_2\text{O}$ showing octahedra forming prismatic slabs separated by the intercalating A layers. (b) Magnetic lattice viewed along the c axis. Cyan and magenta colors denote V atoms on two magnetic sublattices. J_1 , $J_{2\alpha}$, $J_{2\beta}$, J_3 : exchange parameters. (c) AM bulk ordering: all ILL layers are stacked ferromagnetically. (d) AF bulk ordering: ILL layers are stacked antiferromagnetically. A and Q atoms are omitted for clarity in panels (c) and (d). J_\perp : interlayer magnetic coupling.

$\text{AV}_2\text{Q}_2\text{O}$ compounds were taken from the OpenMX distribution. For the self-consistent calculations, the energy cutoff for numerical grid integration was set to 300 Ry, and a $15 \times 15 \times 5$ Monkhorst-Pack k -point mesh was used for Brillouin zone sampling.

The in-plane exchange constants were obtained [20] using the Green’s function-based linear-response technique [39] implemented in OpenMX [35], using the alternating magnetic state as a reference configuration. On the other hand, the interlayer coupling J_\perp was found using the total energy difference, $J_\perp = (E_{\text{FM}} - E_{\text{AFM}})/8$, between the AM and AF orderings within the doubled unit cell, shown in Figs. 1(c) and 1(d). The total energies were calculated using the Vienna Ab initio Simulation Package (VASP) [40–42], within the PBE generalized gradient approximation, using a $24 \times 24 \times 7$ k -point mesh to achieve sufficient convergence.

The results reported in the following were obtained without spin-orbit coupling; we verified for selected cases that its inclusion had a negligible effect on the relevant energy differences. For selected materials we have also evaluated J_\perp using the all-electron package Wien2k [43]; the results were consistent with those obtained in VASP.

Intralayer Exchange Coupling — The calculated intralayer exchange coupling parameters are listed in Table I.

TABLE I: Calculated exchange parameters (meV).

Compound	J_1	$J_{2\alpha}$	$J_{2\beta}$	J_3	J_4	J_\perp
KV ₂ S ₂ O	39.10	35.94	2.78	6.78	-0.16	0.530
KV ₂ Se ₂ O	41.56	34.06	0.84	7.00	-0.16	0.554
KV ₂ Te ₂ O	40.28	31.36	-2.88	6.82	-1.24	0.383
RbV ₂ S ₂ O	39.62	33.20	4.48	7.00	0.14	0.350
RbV ₂ Se ₂ O	44.80	26.22	-1.42	7.54	-1.10	0.339
RbV ₂ Te ₂ O	40.36	29.94	-2.58	6.92	-1.08	0.197
CsV ₂ S ₂ O	41.22	32.06	2.46	7.20	0.10	0.246
CsV ₂ Se ₂ O	42.64	30.80	0.88	7.34	-0.14	0.217
CsV ₂ Te ₂ O	42.48	27.92	-2.04	6.94	1.62	-0.080

As explained in Ref. 20, the magnetic phase stability in an ILL layer may be inferred from the magnetic phase diagram in the $(J_{2\alpha}/|J_1|, J_{2\beta}/|J_1|)$ parameter space, which is shown in Fig. 2.

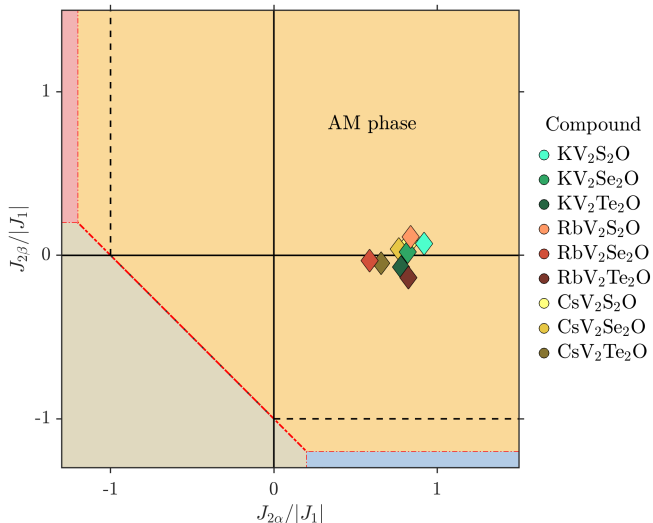


FIG. 2: Magnetic phase diagram in the $(J_{2\alpha}/|J_1|, J_{2\beta}/|J_1|)$ parameter space. The red lines denote the phase boundaries for $J_3 = 0.1|J_1|$. For comparison, black dashed lines show the phase boundaries at $J_3 = 0$ (note that $J_3 > 0$ expands the AM region). The unlabeled regions are various non-AM phases, as discussed in Ref. 20.

As seen from Table I, all compounds exhibit large antiferromagnetic J_1 and ferromagnetic $J_{2\alpha}$ of a comparable magnitude; both these strong couplings favor the AM state. An interesting trend observed across a wider range of compounds [20] is that $J_{2\beta}$ rarely acts as the deciding factor for the in-plane ordering; it is typically either FM or weakly AF. Here, in AV₂Q₂O compounds, it is quite small, and its effect on the magnetic stability is negligible. In contrast, it is more common to find $J_{2\alpha}$ to be strongly AF, leading to 90° noncollinear states as found in La₂O₃Co₂Se₂ [44] and La₂O₃Fe₂Se₂ [45, 46]. In these compounds, the continuous frustration at the

Heisenberg level results in ground states that are determined by higher-order interactions.

The effect of longer-range interactions (beyond J_2) may be included as phase boundary shifts in Fig. 2. Table I shows the J_3 coupling is ferromagnetic in all compounds, providing additional stabilization for the AM state. Surprisingly, J_3 is remarkably similar across distinct compounds, suggesting that this coupling is insensitive to local chemical variations and may be governed by more universal electronic or structural features common to the series. The J_4 parameter is negligibly small, indicating that more distant magnetic couplings have no effect on the magnetic ground state. This validates the truncation of the Heisenberg model at third-nearest neighbors. Overall, the analysis of the exchange coupling confirms that the *intralayer* magnetic order in all studied AV₂Q₂O compounds is reliably AM.

Interlayer Coupling and the Bulk Ground State —

While the preceding discussion of intralayer exchange coupling shows that AM ordering is strongly favored within each layer, the three-dimensional magnetic ground state depends critically on the interlayer coupling J_\perp between the adjacent ILL layers, which are also listed in Table I. We find that nearly all compounds in this family, with the single exception of CsV₂Te₂O, favor AF interlayer stacking.

The preference for AF interlayer stacking has profound consequences for the magnetic symmetry. Such stacking doubles the magnetic unit cell along the c -axis, turning the compound into a conventional, Kramers-denegate antiferromagnet despite satisfying the necessary intralayer conditions for altermagnetism. In this configuration, the two spin sublattices between different layers can be mapped onto each another through a lattice translation, violating the symmetry requirements for altermagnetism [2].

Thus, while vanadium-based ILL compounds remain promising for hosting altermagnetism within single layers, bulk altermagnetism requires careful attention to interlayer ordering. Among the nine compounds considered here, only CsV₂Te₂O appears to be suitable, based on our DFT calculations.

In this connection, it is interesting to revisit a related Sr₂CrO₂Cr₂OAs₂ ILL compound, which was shown in Ref. 20 to host robust AM order within its Cr-based ILL layers. That compound also has a high T_N and is metallic with a highly anisotropic d -wave Fermi surface. In contrast to other known ILL-based oxychalcogenides, the ILL layers in Sr₂CrO₂Cr₂OAs₂ alternate with perovskite-like CrO₂ layers, which, taken individually, are not AM. Nevertheless, the bulk compound belongs to an AM spin group. We emphasize that this AM character does not depend on whether the interlayer ordering is FM or AF, because in either case the magnetic unit cell contains only one ILL layer.

Influence of Charge Doping on Exchange Coupling —

Given that most stoichiometric AV_2Q_2O compounds exhibit weak AF interlayer coupling, it is natural to examine whether this coupling is sensitive to charge doping. Indeed, some compounds in this family, such as $Rb_{1-\delta}V_2Te_2O$ [19, 28], could exhibit intrinsic hole doping due to alkali metal deficiency.

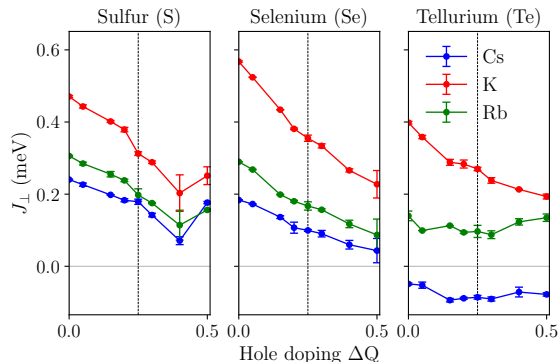


FIG. 3: Interlayer exchange coupling J_{\perp} as a function of hole doping ΔQ (per f.u.). $\Delta Q = 0$ corresponds to the stoichiometric composition. The error bars show the difference between the calculations performed with $26 \times 26 \times 7$ and $22 \times 22 \times 7$ k -point meshes.

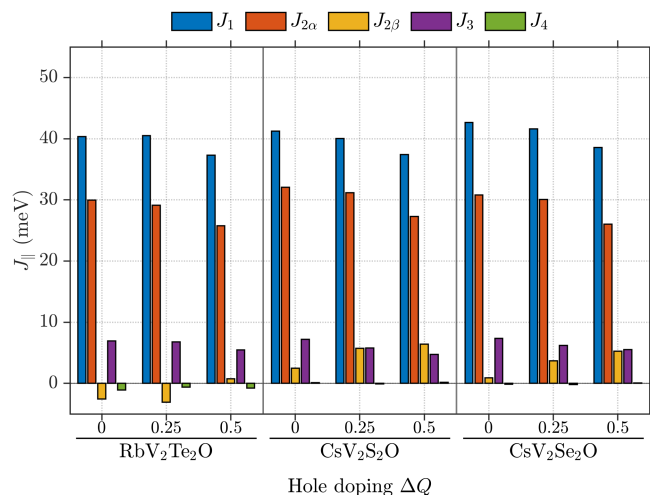


FIG. 4: Dependence of the intralayer exchange parameters on hole doping ΔQ (holes per f.u.) for selected compounds.

The hole-doping dependence of the interlayer exchange coupling J_{\perp} is shown in Fig. 3.

We observe monotonic decline in J_{\perp} as the filler layer changes from K to Rb to Cs while the chalcogen element remains the same. This systematic trend is most likely due to the significant increase in the interlayer spacing as larger alkali metal cations are incorporated into the structure.

We also observe monotonic decline in J_{\perp} under doping of up to 0.25 holes per formula unit. K-based compounds (red lines in Fig. 3) show the steepest decline but remain strongly positive. Rb-based compounds (green lines) also show weakening of J_{\perp} , but in tellurides this trend is much weaker. In Cs-based compounds with S and Se (blue lines), J_{\perp} first decreases strongly and then tends to saturate, remaining positive up to 0.5 holes per f.u. In CsV_2Te_2O , which is the only case with $J_{\perp} < 0$ at stoichiometry, hole doping has no significant effect on J_{\perp} . Thus, hole doping within a reasonable range does not change the sign of J_{\perp} in any of the studied compounds.

Figure 4 shows that intralayer exchange parameters are rather insensitive to hole doping, implying that intralayer AM order is also stable under moderate deviations from stoichiometry.

Conclusions — Our systematic study of nine vanadium-based oxychalcogenide inverse Lieb-lattice compounds suggests that all except one of them have a conventional antiferromagnetic ground state with the doubled magnetic unit cell along the c axis. The only exception is CsV_2Te_2O , which is predicted to be AM in the bulk and appears to be the prime candidate for experimental verification. This conclusion is not affected by doping of up to 0.5 holes per formula unit.

* bthapa3@gmu.edu

† pchang8@gmu.edu

‡ belashchenko@unl.edu

§ imazin2@gmu.edu

- [1] I. Mazin, *Phys. Rev. X* **12**, 040002 (2022).
- [2] L. Šmejkal, J. Sinova, and T. Jungwirth, *Phys. Rev. X* **12**, 031042 (2022).
- [3] I. I. Mazin, K. Koepf, M. D. Johannes, R. González-Hernández, and L. Šmejkal, *Proceedings of the National Academy of Sciences* **118**, e2108924118 (2021).
- [4] L. Šmejkal, A. H. MacDonald, J. Sinova, S. Nakatsuji, and T. Jungwirth, *Nature Reviews Materials* **7**, 482 (2022).
- [5] L. Šmejkal, A. B. Hellènes, R. González-Hernández, J. Sinova, and T. Jungwirth, *Phys. Rev. X* **12**, 011028 (2022).
- [6] L. Šmejkal, J. Sinova, and T. Jungwirth, *Phys. Rev. X* **12**, 040501 (2022).
- [7] L. Bai, W. Feng, S. Liu, L. Šmejkal, Y. Mokrousov, and Y. Yao, *Advanced Functional Materials* **34**, 2409327 (2024).
- [8] X. Zhang, P. Jiang, L.-Y. Xu, L. Wang, L. Liu, H.-M. Huang, T. Cao, and Y.-L. Li, *Nano Letters* **25**, 16547 (2025).
- [9] X. Yang, S.-S. Wang, and S. Dong, *Advanced Functional Materials*, 17921 (2025).
- [10] R. González-Hernández, L. Šmejkal, K. Vyborný, Y. Yahagi, J. Sinova, T. Jungwirth, and J. Železný, *Physical Review Letters* **126**, 127701 (2021).
- [11] A. Bose, N. J. Schreiber, R. Jain, D.-F. Shao, H. P. Nair, J. Sun, X. S. Zhang, D. A. Muller, E. Y. Tsymb-

- bal, D. G. Schlom, and D. C. Ralph, *Nature Electronics* **5**, 267 (2022).
- [12] H. Bai, L. Han, X. Y. Feng, Y. J. Zhou, R. X. Su, Q. Wang, L. Y. Liao, W. X. Zhu, X. Z. Chen, F. Pan, *et al.*, *Physical Review Letters* **128**, 197202 (2022).
- [13] D.-F. Shao, S.-H. Zhang, M. Li, C.-B. Eom, and E. Y. Tsymbal, *Nature Communications* **12**, 7061 (2021).
- [14] S. Karube, T. Tanaka, D. Sugawara, N. Kadoguchi, M. Kohda, and J. Nitta, *Physical Review Letters* **129**, 137201 (2022).
- [15] N. Kaushal and M. Franz, *arXiv e-prints*, [arXiv:2412.16421](https://arxiv.org/abs/2412.16421) (2024), [arXiv:2412.16421](https://arxiv.org/abs/2412.16421) [cond-mat.str-el].
- [16] M. Dürnagel, H. Hohmann, A. Maity, J. Seufert, M. Klett, L. Klebl, and R. Thomale, *Phys. Rev. Lett.* **135**, 036502 (2025).
- [17] C.-C. Wei, X. Li, S. Hatt, X. Huai, J. Liu, B. Singh, K.-M. Kim, R. M. Fernandes, P. Cardon, L. Zhao, T. T. Tran, B. A. Frandsen, K. S. Burch, F. Liu, and H. Ji, *Physical Review Materials* **9**, 024402 (2025).
- [18] B. Jiang, M. Hu, J. Bai, Z. Song, C. Mu, G. Qu, W. Li, W. Zhu, H. Pi, Z. Wei, Y. Sun, Y. Huang, X. Zheng, Y. Peng, L. He, S. Li, J. Luo, Z. Li, G. Chen, H. Li, H. Weng, and T. Qian, *Nature Physics* **21**, 754 (2025).
- [19] F. Zhang, X. Cheng, Z. Yin, C. Liu, L. Deng, Y. Qiao, Z. Shi, S. Zhang, J. Lin, Z. Liu, M. Ye, Y. Huang, X. Meng, C. Zhang, T. Okuda, K. Shimada, S. Cui, Y. Zhao, G.-H. Cao, S. Qiao, J. Liu, and C. Chen, *Nature Physics* **21**, 760 (2025).
- [20] P.-H. Chang, I. I. Mazin, and K. D. Belashchenko, *Inverse Lieb Materials: Altermagnetism and More* (2025), [arXiv:2508.04839](https://arxiv.org/abs/2508.04839) [cond-mat].
- [21] S. Zeng and Y.-J. Zhao, *Phys. Rev. B* **110**, 054406 (2024).
- [22] D. B. Litvin and W. Opechowski, *Physica* **76**, 538 (1974).
- [23] W. F. Brinkman and R. J. Elliott, *Proceedings of the Royal Society of London. Series A: Mathematical and Physical Sciences* **294**, 343 (1966).
- [24] L. Garcia-Gassull, A. Razpopov, P. P. Stavropoulos, I. I. Mazin, and R. Valentí, *arXiv e-prints*, [arXiv:2506.21661](https://arxiv.org/abs/2506.21661) (2025), [arXiv:2506.21661](https://arxiv.org/abs/2506.21661) [cond-mat.str-el].
- [25] H. Lin, J. Si, X. Zhu, K. Cai, H. Li, L. Kong, X. Yu, and H.-H. Wen, *Physical Review B* **98**, 075132 (2018).
- [26] Y.-X. Yu, *Applied Surface Science* **546**, 149062 (2021).
- [27] H.-Y. Ma, M. Hu, N. Li, J. Liu, W. Yao, J.-F. Jia, and J. Liu, *Nature Communications* **12**, 2846 (2021).
- [28] A. Ablimit, Y.-L. Sun, H. Jiang, S.-Q. Wu, Y.-B. Liu, and G.-H. Cao, *Physical Review B* **97**, 214517 (2018).
- [29] Y. Zhu, T. Chen, Y. Li, L. Qiao, X. Ma, C. Liu, T. Hu, H. Gao, and W. Ren, *Nano Letters* **24**, 472 (2024).
- [30] K. Zou, Y. Yang, B. Xin, W. Wu, Y. Cheng, H. Dong, H. Liu, F. Luo, F. Lu, and W.-H. Wang, *Journal of Physics: Condensed Matter* **37**, 055804 (2024), publisher: IOP Publishing.
- [31] N. D. Kelly and S. J. Clarke, *Journal of Solid State Chemistry* **327**, 124276 (2023).
- [32] M. Valldor, P. Merz, Y. Prots, and W. Schnelle, *European Journal of Inorganic Chemistry* **10.1002/ejic.201501154** (2016).
- [33] Y. Sun, Y. Huang, J. Cheng, S. Zhang, Z. Li, H. Luo, X. Ma, W. Yang, J. Yang, D. Chen, K. Sun, M. Gutmann, S. C. Capelli, F. Shen, J. Hao, L. He, G. Chen, and S. Li, *Phys. Rev. B* **112**, 184416 (2025).
- [34] T. Ozaki, *Phys. Rev. B* **67**, 155108 (2003).
- [35] T. Ozaki, H. Kino, J. Yu, M. Han, M. Ohfuchi, F. Ishii, K. Terakura, K. Sawada, Y. Kubot, Y. Mizuta, *et al.*, The code OPENMX pseudoatomic basis functions, and pseudopotentials are available under terms of the GNU-GPL on a web site, <http://www.openmx-square.org/> (2016).
- [36] I. Morrison, D. M. Bylander, and L. Kleinman, *Physical Review B* **47**, 6728 (1993).
- [37] D. Vanderbilt, *Physical Review B* **41**, 7892 (1990).
- [38] J. P. Perdew, K. Burke, and M. Ernzerhof, *Phys. Rev. Lett.* **77**, 3865 (1996).
- [39] V. Antropov, M. Katsnelson, and A. Liechtenstein, *Physica B: Condensed Matter* **237–238**, 336 (1997).
- [40] G. Kresse and J. Hafner, *Phys. Rev. B* **47**, 558 (1993).
- [41] G. Kresse and J. Furthmüller, *Computational Materials Science* **6**, 15 (1996).
- [42] G. Kresse and J. Furthmüller, *Phys. Rev. B* **54**, 11169 (1996).
- [43] P. Blaha, K. Schwarz, G. K. H. Madsen, D. Kvasnicka, and J. Luitz, WIEN2K (2002), ISBN 3-9501031-1-2.
- [44] Y. Fuwa, T. Endo, M. Wakeshima, Y. Hinatsu, and K. Ohoyama, *Journal of the American Chemical Society* **132**, 18020 (2010).
- [45] M. Günther, S. Kamusella, R. Sarkar, T. Goltz, H. Luetkens, G. Pascua, S.-H. Do, K.-Y. Choi, H. D. Zhou, C. G. F. Blum, S. Wurmehl, B. Büchner, and H.-H. Klauss, *Physical Review B* **90**, 184408 (2014).
- [46] E. E. McCabe, C. Stock, E. E. Rodriguez, A. S. Wills, J. W. Taylor, and J. S. O. Evans, *Physical Review B* **89**, 100402 (2014).